Supporting Information

Tuning the Ground State and Excited State Properties of Monocationic Iridium(III) Complexes by Varying the Site of Benzannulation on Diimine Ligand

Bingqing Liu, Levi Lystrom, Svetlana Kilina and Wenfang Sun*

Department of Chemistry and Biochemistry, North Dakota State University, Fargo, North Dakota 58108-6050, United States

Table S1. Natural transition orbitals (NTOs) representing singlet transitions contributing to the low-energy absorption bands of **1-6** in CH_2Cl_2.

	S_n	Hole	Electron			Hole	Electron
1	S_1 527 nm f = 0.001	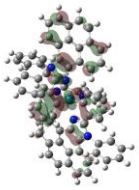		**4**	S_1 545 nm f = 0.006	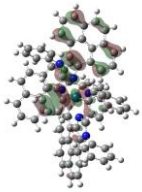	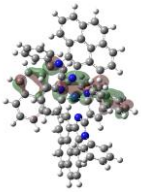
	S_2 494 nm f = 0.002	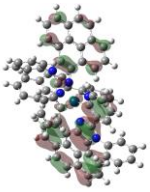	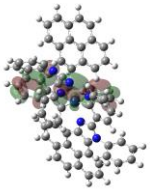		S_2 513 nm f = 0.017	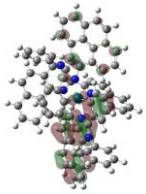	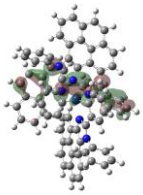
	S_3 440 nm f = 0.002	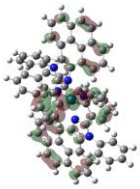	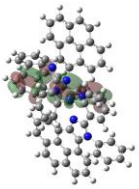		S_3 454 nm f = 0.015	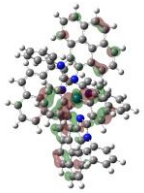	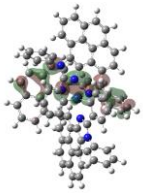
2	S_1 501 nm f = 0.005	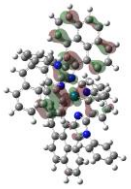	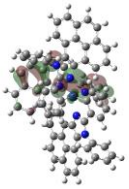	**5**	S_1 583 nm f = 0.001	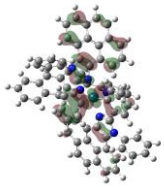	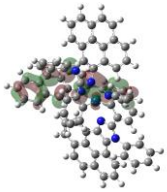
	S_2 466 nm f = 0.007	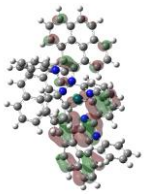	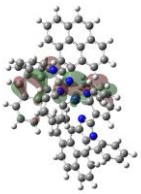		S_2 542 nm f = 0.002	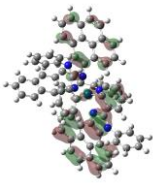	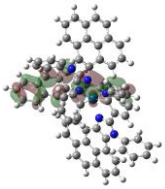
	S_3 420 nm f = 0.010	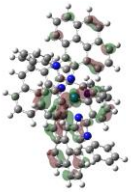	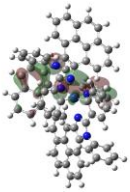		S_3 476 nm f = 0.004	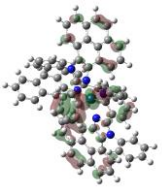	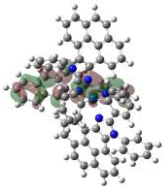
	S_4 401 nm f = 0.104	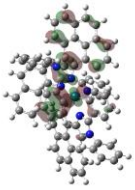	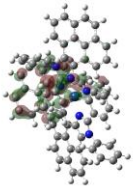		S_4 453 nm f = 0.060	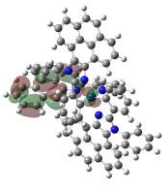	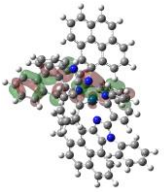
3	S_1 570 nm f = 0.010	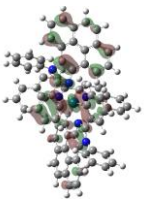	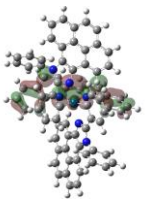	**6**	S_1 612 nm f = 0.012	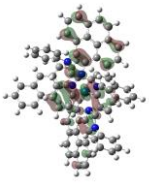	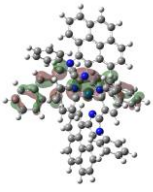

S_2 540 nm f = 0.019	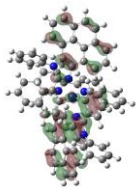	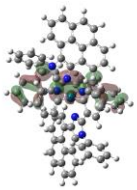	S_2 581 nm f = 0.145	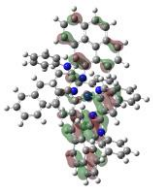	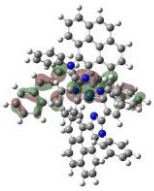
S_3 468 nm f = 0.011	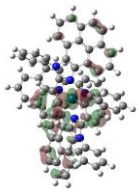	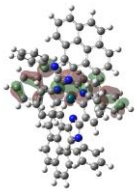	S_3 498 nm f = 0.267	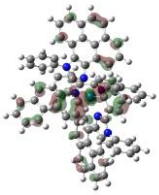	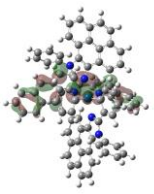
S_4 425 nm f = 0.031	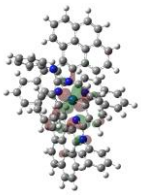	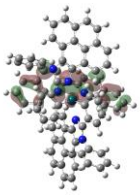	S_4 484 nm f = 0.024	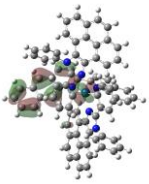	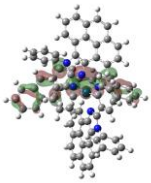
S_5 420 nm f = 0.034	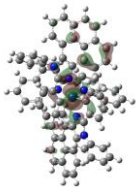	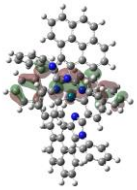	S_5 444 nm f = 0.010	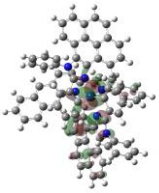	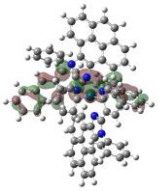
			S_6 439 nm f = 0.015	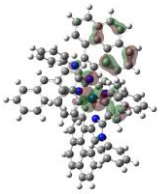	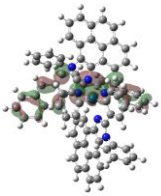

Table S2. Characterization of molecular orbitals for the first five HOMOs and LUMOs of **1-6** in CH_2Cl_2

	1	**2**	**3**	**4**
LUMO+4	π*(C^N)	π*(C^N)/*d*(Ir)	π*†	π*†
LUMO+3	π*(C^N-N^N)	π*(C^N)	π*(C^N)	π*(N)
LUMO+2	π*(C^N)	π*(pyr)	π*(C^N)	π*†
LUMO+1	π*(C^N)	π*†	π*(N^N)	π*(N^N)/π*(Ph)
LUMO	π*(N^N)	π*(N^N)	π*(N^N)/ *d*(Ir)	π*(N^N)
HOMO	*d*(Ir)/ π(C^N)	*d*(Ir)/ π(C^N)	*d*(Ir)/ π(C^N)	*d*(Ir)/ π(C^N)
HOMO-1	π(C^N)/*d*(Ir)	π(C^N)	π(C^N)	π(C^N)
HOMO-2	*d*(Ir)/ π(C^N)	π†	*d*(Ir)/ π(C^N)	*d*(Ir)/ π(C^N)
HOMO-3	*d*(Ir)/ π(C^N)	π†	*d*(Ir)/ π(C^N)	π†
HOMO-4	*d*(Ir) / π(C^N)	π†	*d*(Ir)/ π(C^N)	*d*(Ir)/ π(C^N)

	5	**6**
LUMO+4	π*(C^N)	π*(N^N) / *d*(Ir)
LUMO+3	π*(C^N)	π*(C^N)
LUMO+2	π*(C^N)	π*(C^N)
LUMO+1	π*(C^N-N^N)	π*(N^N)
LUMO	π*(N^N) / *d*(Ir)	π*(N^N) / *d*(Ir)
HOMO	*d*(Ir)/ π(C^N)	π(C^N)/ *d*(Ir)
HOMO-1	π(C^N) / *d*(Ir)	π(C^N)
HOMO-2	*d*(Ir)/ π(C^N)	π(N)/*d*(Ir)/π(C^N)
HOMO-3	π(C^N) / *d*(Ir)	*d*(Ir)/π(C^N)/π(N)
HOMO-4	π(C^N) / *d*(Ir)	*d*(Ir)/π(C^N)/π(N)

Table S3. HOMOs and LUMOs of **1-6** in CH_2Cl_2

	HOMO	LUMO		HOMO	LUMO	
1	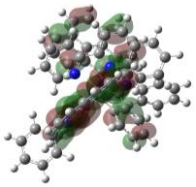	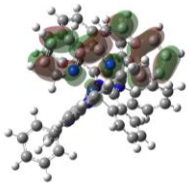	**2**	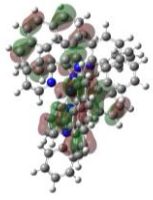	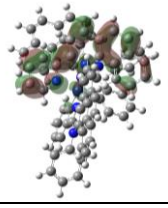	H-L[a]
1	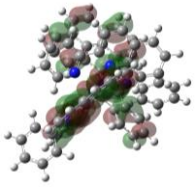	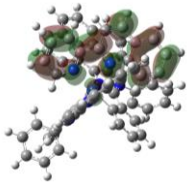	**3**	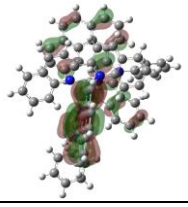	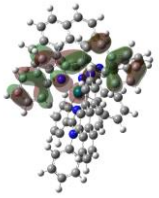	L-L[b]
1	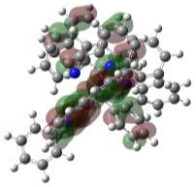	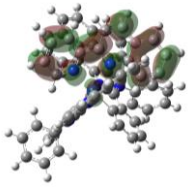	**5**	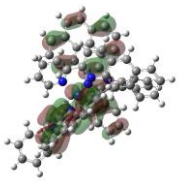	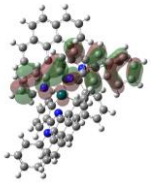	L-L[b]
5	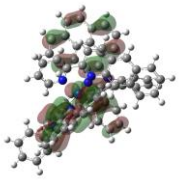	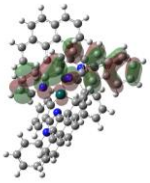	**6**	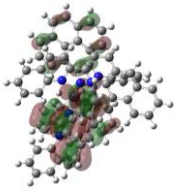	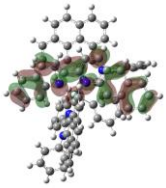	L-L[b]
3	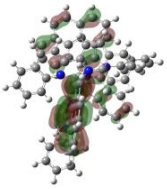	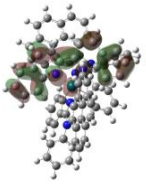	**6**	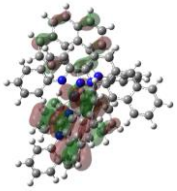	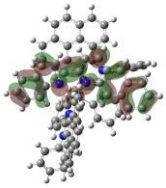	L-L[b]
2	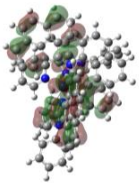	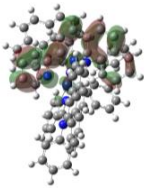	**4**	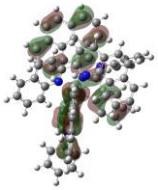	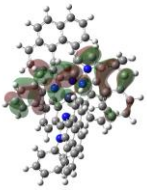	L-L[b]
3	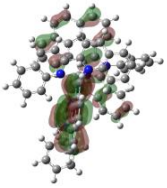	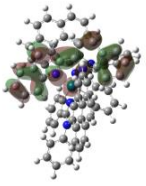	**4**	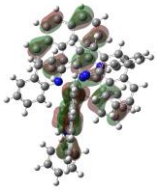	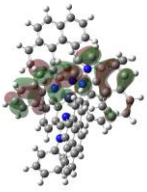	H-L[a]
	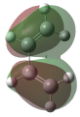	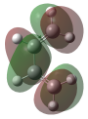				

[a] H-L indicates the interactions between the HOMOs of **1** or **3** with the LUMO of 1,3-butadiene to give the LUMOs of **2** and **4**. [b] L-L indicates the interactions between the LUMOs of **1**, **3** or **5** with the LUMO of 1,3-butadiene to give the LUMOs of **3**, **5** and **6**.

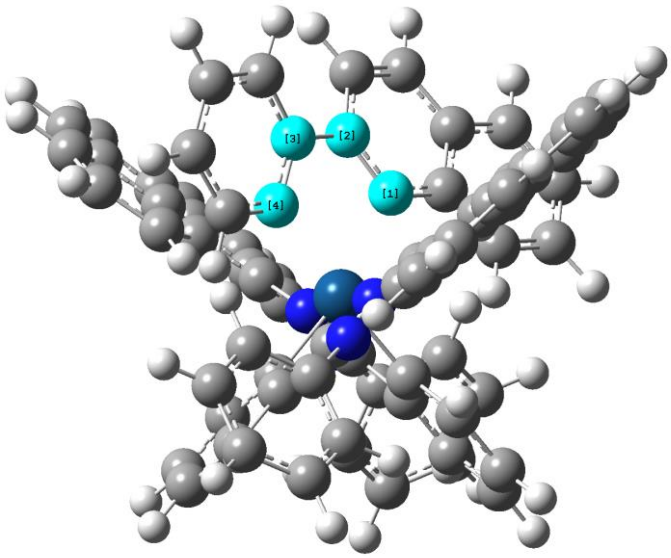

Table S4. Dihedral angle on the N^N ligand obtained from the optimized ground-state geometry of **1-6** in CH_2Cl_2

	Torque angle
1	19.9°
2	27.9°
3	18.9°
4	29.1°
5	19.8°
6	18.7°

Table S5. Percentage of HOMO-LUMO transition contributing to S_1 of **1-6** calculated in CH_2Cl_2 solvent.

	Percent HOMO-LUMO
1	67%
2	68%
3	64%
4	68%
5	67%
6	64%

Table S6. NTOs representing transitions corresponding to the triplet emission of **1**−**6** in CH_2Cl_2 calculated by the second method, TDDFT-based ΔSCF. Energies obtained from the first method, ΔSCF, are shown in parenthesis.

Complexes	T_1 / nm	Hole	Electron
1	671 (656)	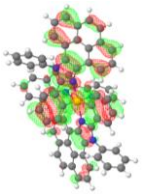	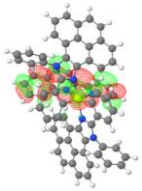
2	645 (638)	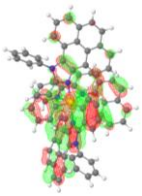	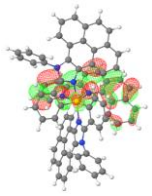
3	733 (714)	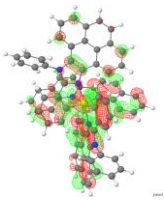	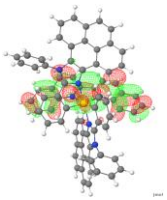
4	735 (702)	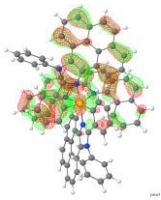	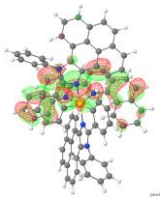
5	1356 (765)	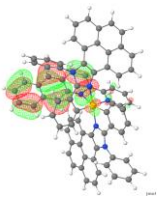	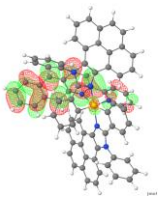
6	1398 (804)	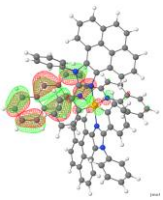	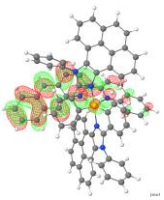

Table S7. Emission characteristics of complexes **1**−**6** in different solvents at room temperature [a]

λ_{em}/nm (τ_{em}/μs); Φ_{em}				
	CH_3CN	THF	CH_2Cl_2	Toluene (with 10% CH_2Cl_2)
1	628 (0.68); 0.06	624 (0.84); 0.13	625 (0.94); 0.13	622 (0.47); 0.08
2	600 (-)[b]; 0.0089	600 (-)[b]; 0.0097	593 (0.15); 0.017	598 (-)[b]; 0.0096
3	663 (0.45); 0.049	657 (0.58); 0.057	657 (0.93); 0.12	672 (0.20); 0.020
4	-[b]	645 (1.29); 0.041	645 (1.34); 0.085	645 (0.36); 0.030
5	735 (2.11); 0.0028	739 (1.95); 0.0039	740 (2.21); 0.0049	731 (2.01); 0.0045
6	766 (0.71); 0.0024	765 (0.87); 0.0032	766 (0.86); 0.0039	765 (0.37); 0.0025

[a] $Ru(bpy)_3Cl_2$ in CH_3CN was used as the reference (λ_{ex} = 436 nm, Φ_{em} = 0.097) for the emission quantum yield measurements. The quantum yields for **5** and **6** are just for the emission in the region of 700-850 nm detected by the Hamamatsu photomultiplier tube (PMT) R928. [b] Signal was too weak to be detected.

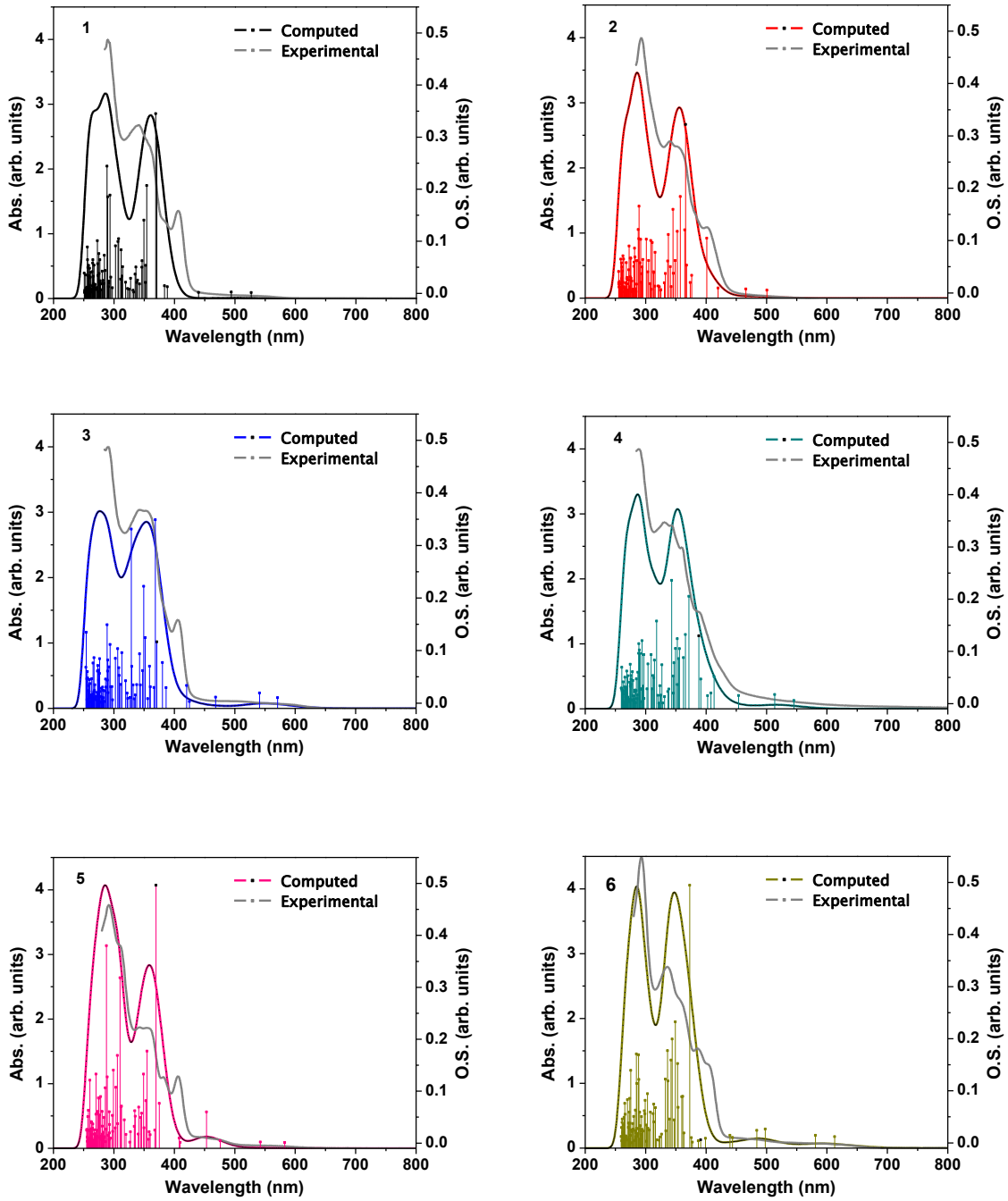

Figure S1. Comparison of the computed and experimental absorption spectra of **1-6** in CH_2Cl_2

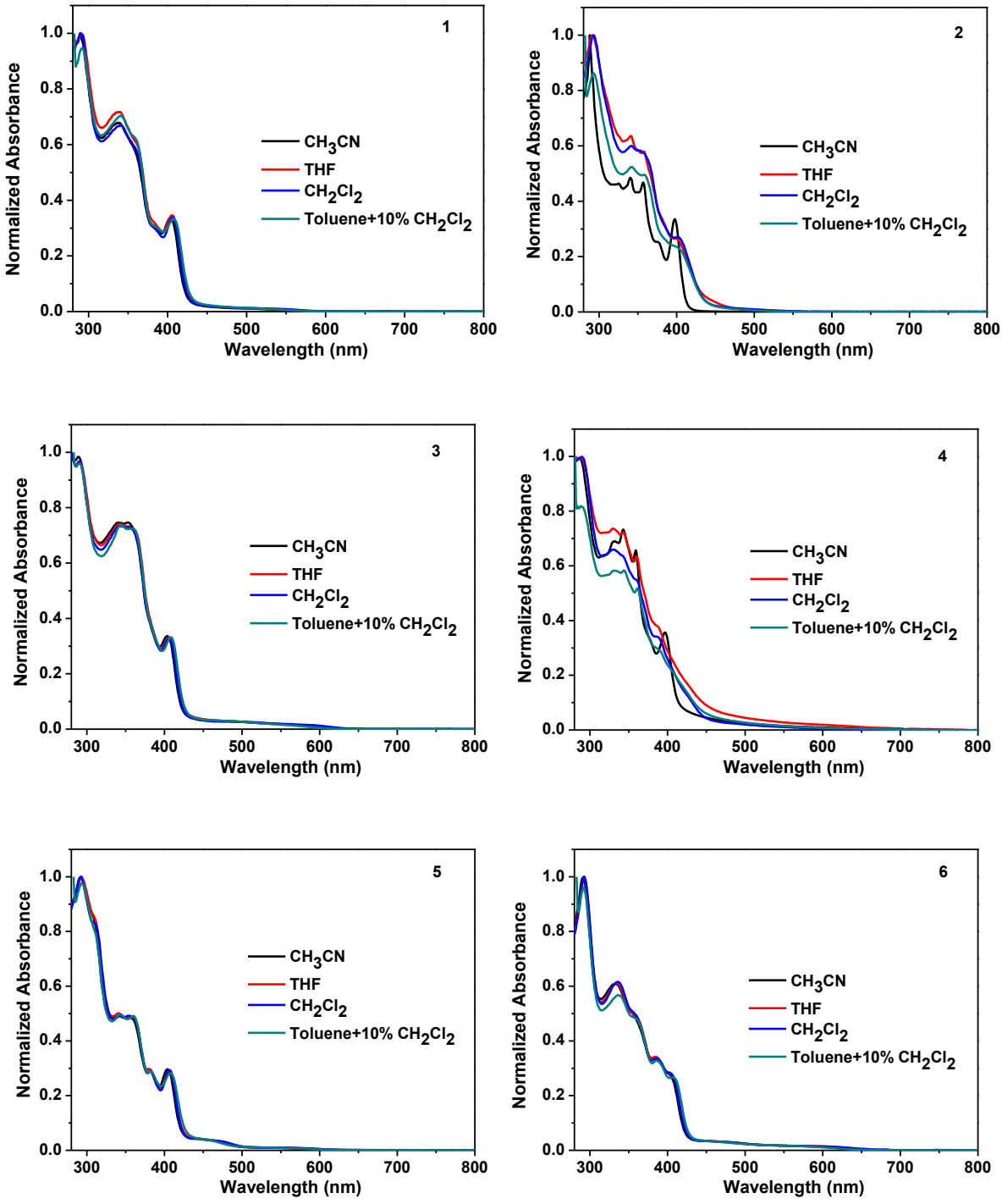

Figure S2. Normalized experimental absorption spectra of **1-6** in different solvents.

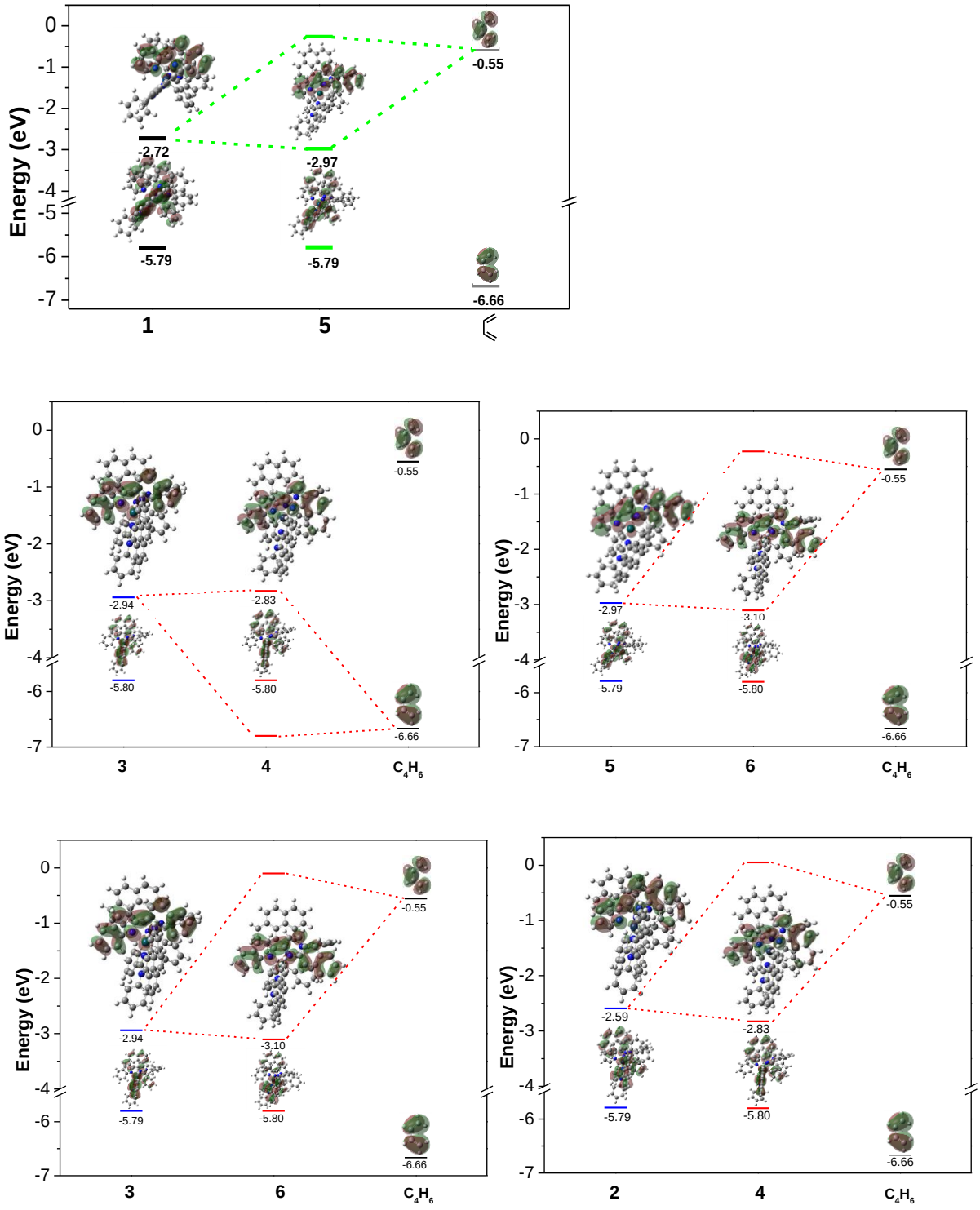

Figure S3. Frontier molecular orbital mixing between **1**, **2**, **3**, **5** and 1,3-butadiene (C_4H_6).

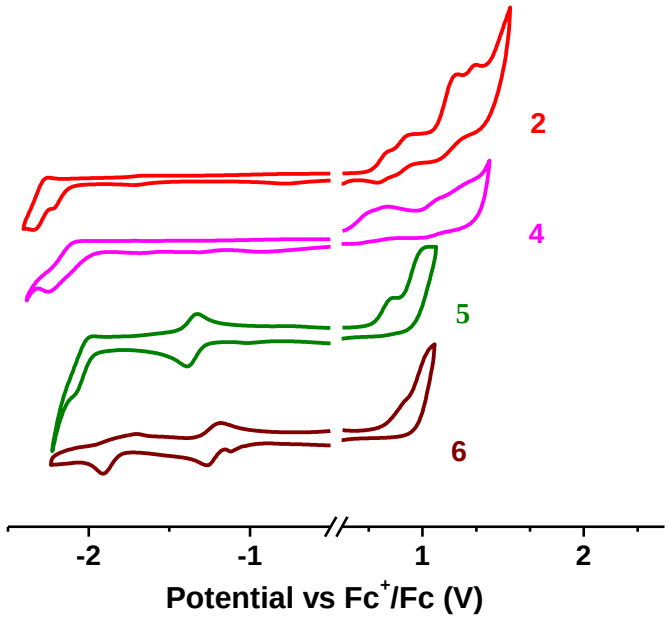

Figure S4. Cyclic voltammograms of complexes **2**, **4**, **5** and **6** in degassed anhydrous CH_3CN solutions (1×10^{-3} M) in the presence of 0.1 M tetrabutylammonium hexafluorophosphate as the supporting electrolyte and ferrocenium/ferrocene (Fc^+/Fc) couple as the internal standard. The potentials were recorded against an Ag/AgCl reference electrode, but are plotted vs the Fc^+/Fc couple.

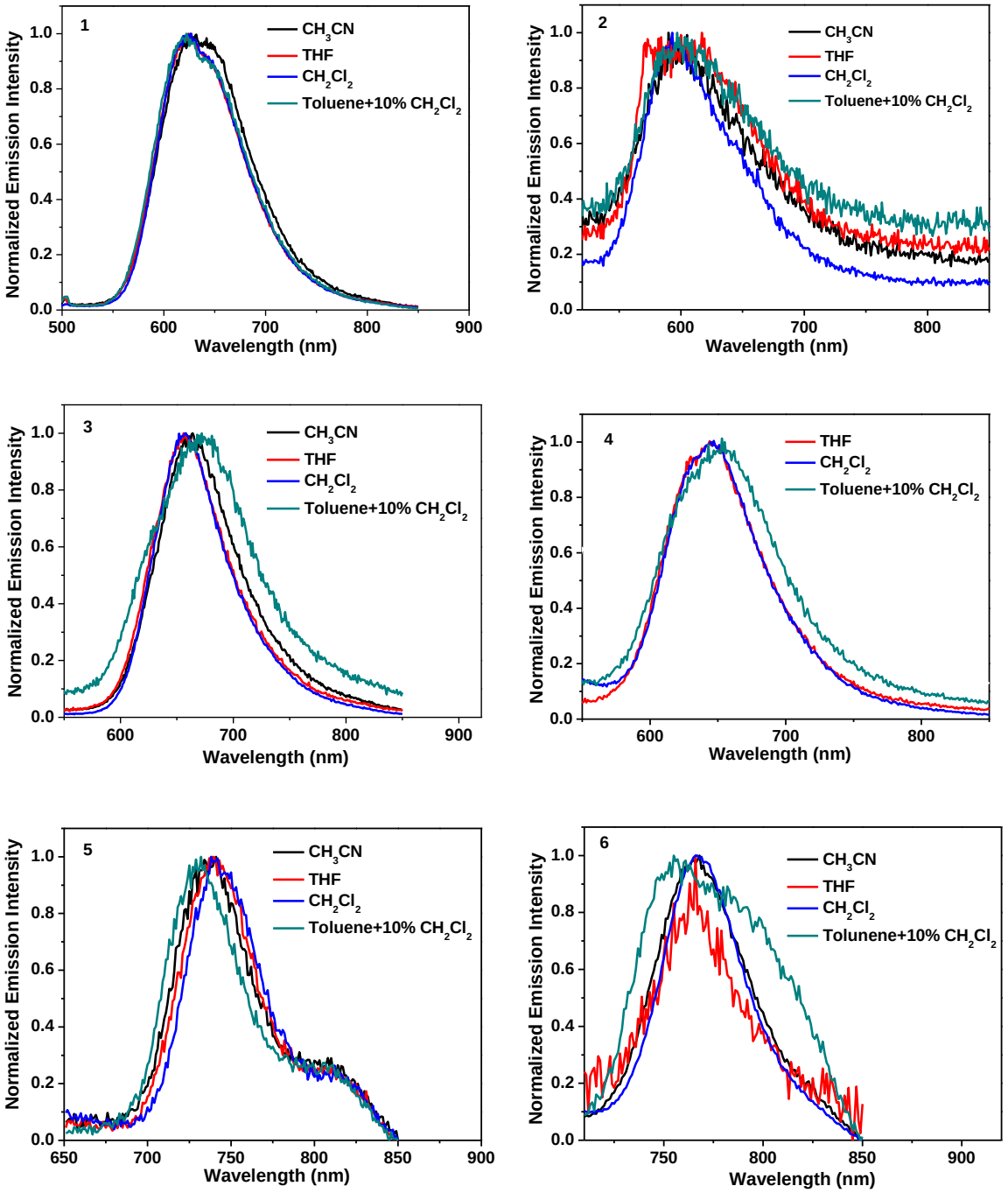

Figure S5. Normalized experimental emission spectra of **1**−**6** at room temperature in different solvents. Hamamatsu R928 PMT was used as the detector for these measurements.

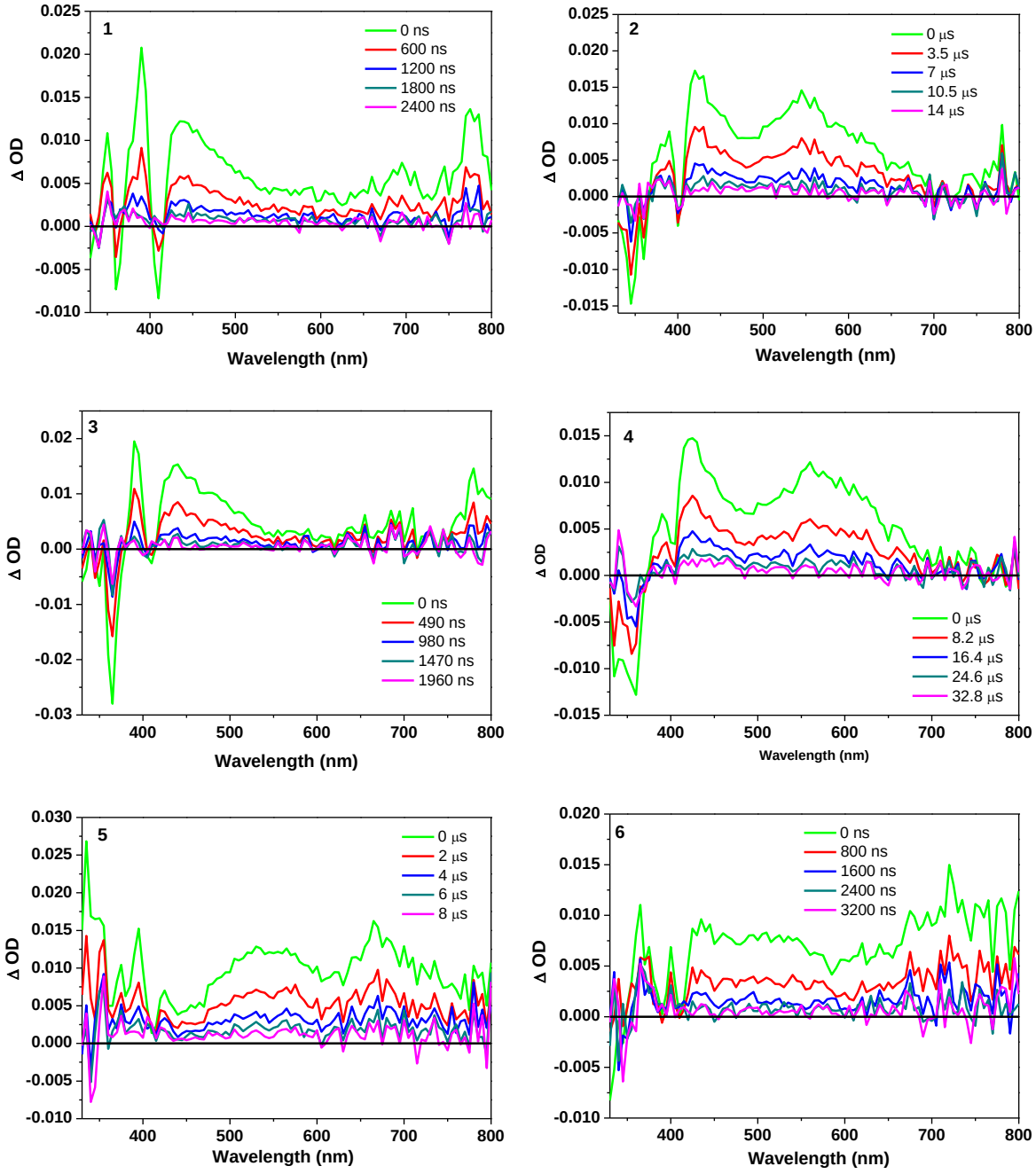

Figure S6. Nanosecond time-resolved transient differential absorption spectra of **1**−**6** in acetonitrile. λ_{ex} = 355 nm, A_{355} = 0.4 in a 1-cm cuvette.

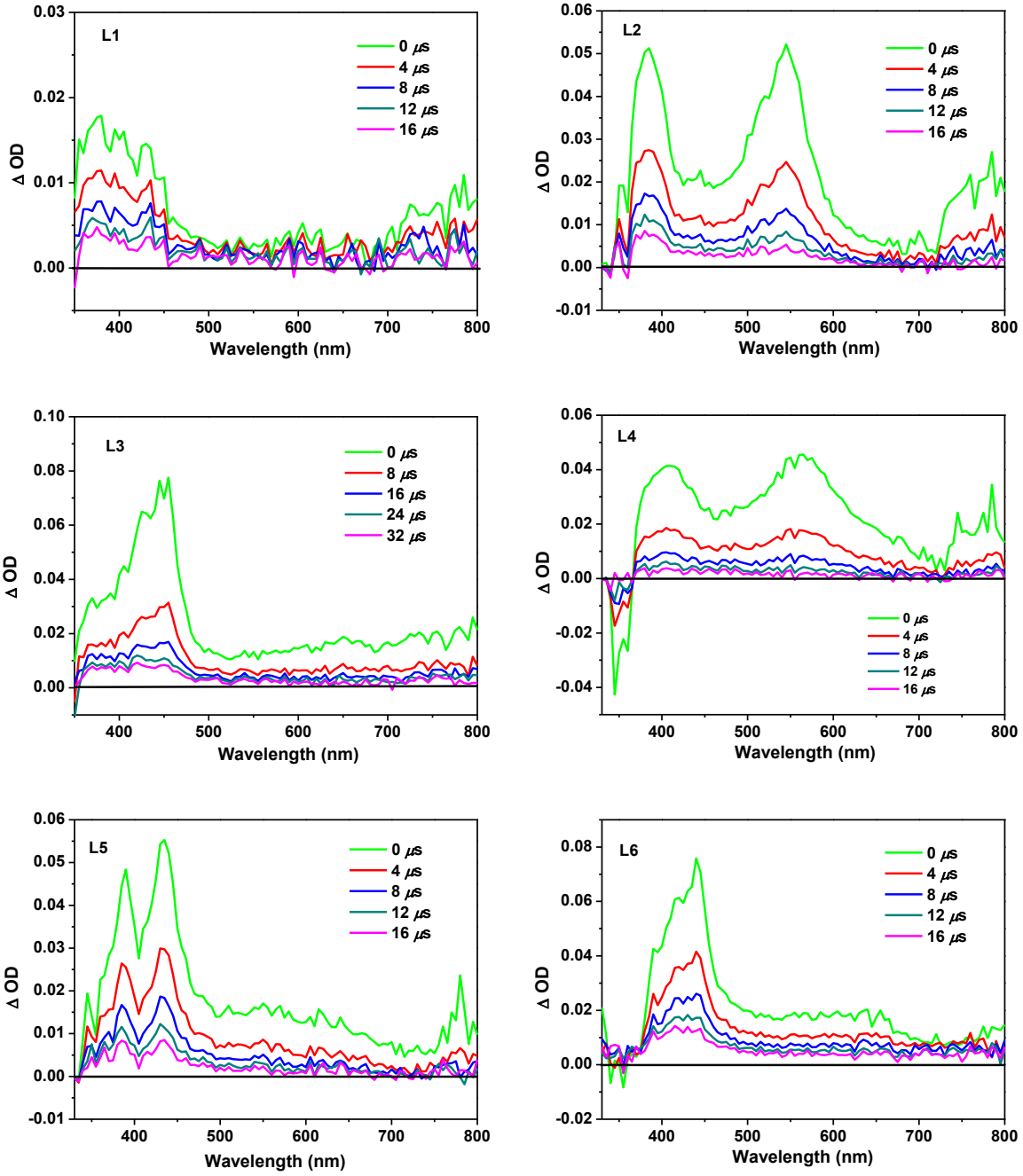

Figure S7. Nanosecond time-resolved transient differential absorption spectra of **L1**−**L6** in acetonitrile. λ_{ex} = 355 nm, A_{355} = 0.4 in a 1-cm cuvette.

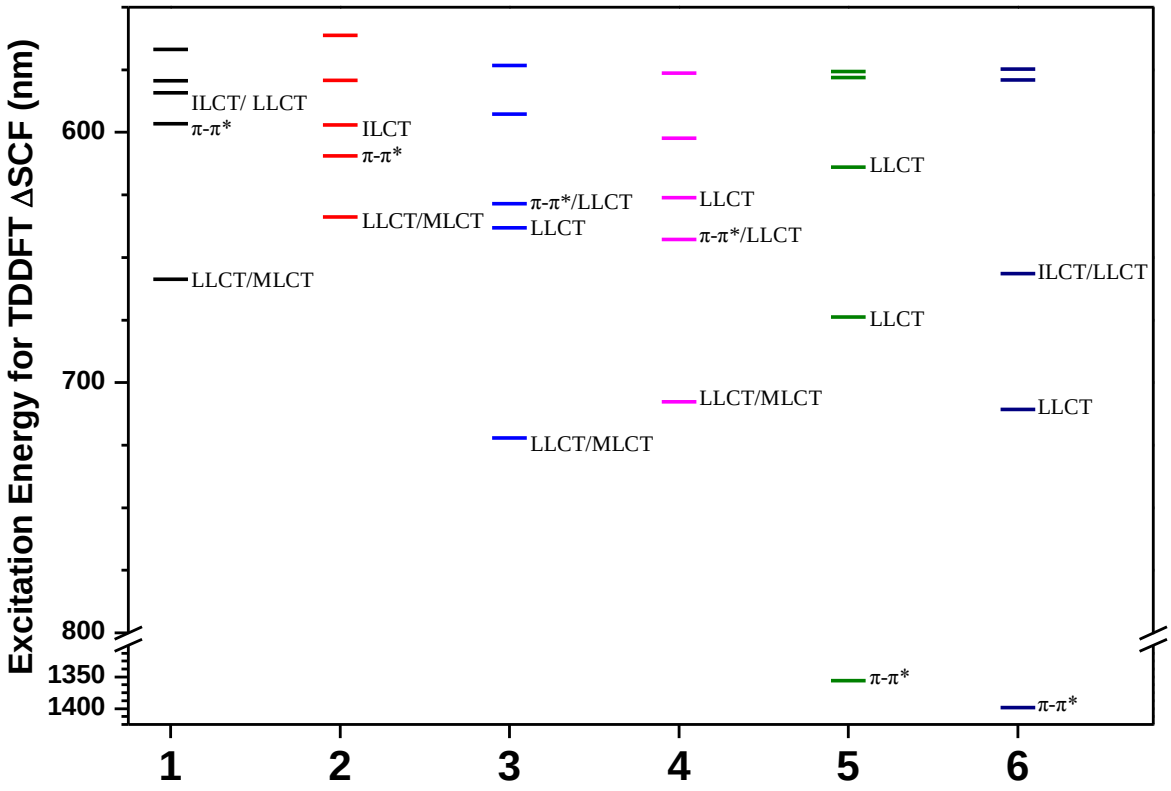

Figure S8. Calculated triplet excited state energy diagram for **1-6** in CH_3CN using the triplet state geometries from the ground state optimization.